PAPER

Check for updates

Amine functionalized 3D porous organic polymer as an effective adsorbent for removing organic dyes and solvents

Yan He,[a] Ting Xu,[a] Jun Hu,[a] Changjun Peng, [ID] *[a] Qiang Yang,*[b] Hualin Wang[b] and Honglai Liu[a]

Organic dyes and solvents are emerging pollutants; the development of new materials for their efficient adsorption and removal is thus of great significance. In this work, we report the application of an amine functionalized triptycene-based 3D polymer (TPP-NH$_2$) as a novel adsorbent for the fast removal of organic dyes in aqueous solution and organic solvents with a view to understanding its adsorption kinetics, adsorption isotherms, desorption and adsorbent regeneration. The adsorption of organic dyes (cationic methylene blue, MEB, and anionic methyl orange, MO) on TPP-NH$_2$ was fast, and most of the dyes were adsorbed in 60 min. The adsorption of MEB and MO follows pseudo-second-order kinetics and fits the Langmuir model, where the maximum adsorption capacity increased from 204.9 mg g^{-1} to 560.6 mg g^{-1} and 213.2 mg g^{-1} to 803.2 mg g^{-1} for MEB and MO, respectively, as the temperature increased, suggesting that the adsorption of MEB and MO on TPP-NH$_2$ is favorable at high temperatures via an endothermic process. The pH has no obvious effect on the adsorption of MEB and MO. The used TPP-NH$_2$ could be regenerated effectively and recycled at least five times without a significant loss of adsorption capacity. In addition, the TPP-NH$_2$ can adsorb up to 33 times its own weight in organic solvents while wiping off the water. The high surface area, hierarchical porosity and $\pi-\pi$ stacking interactions between the aromatic rings of MEB and MO and the aromatic rings of 3D TPP-NH$_2$ were responsible for the efficient adsorption. Therefore, the TPP-NH$_2$ that was synthesized using the facile strategy possesses significant potential in the treatment of wastewater.

1. Introduction

Organic dyes, as important industrial products, have been widely used for the dyeing of silk, cotton, linen and fiber. However, they also have many drawbacks, such as being toxic contaminants, being difficult to degrade and generating lots of pollution.[1–4] So far, there are a few methods reported for removing dyes from aqueous solution, such as physical and chemical methods, biological oxidation, incineration and adsorption.[3–7] Adsorption is considered as a promising method among them because it is highly effective, economical, and the simplest.[3,7–10] However, using traditional porous adsorbents such as activated carbon,[11] zeolites[12] and oriented clay films[10] for the adsorption of dyes gave low adsorption capacities. Therefore, exploring novel adsorbents for the efficient

adsorption and removal of dyes is still of great significance and is challenging.

Recently, porous organic polymers (POPs)[13,14] have emerged as a new type of porous material with diverse applications because of their high surface areas, good porosities and structure diversity. In addition, POPs can be designed and constructed as task-specific materials by introducing multiple chemical functionalities into the porous network.[15–17] A variety of amine functionalized POPs have been synthesized and developed for CO$_2$ capture and metal catalyst support due to their high surface areas, well defined pores and high physicochemical stability.[17,18] In principle, a highly porous polymer with amine functionality should also be an excellent adsorbent for the scavenging and removal of organic dyes and solvents. However, the application of POPs in organic dye and solvent removal has rarely been reported.

Herein, we report the first successful study on the application of an amine functionalized triptycene-based 3D porous polymer TPP-NH$_2$ as a new adsorbent for the fast adsorption and removal of organic dyes with different charges as well as organic solvents, to our knowledge. The adsorption kinetics, adsorption isotherms and the regeneration of the adsorbent for the removal of MEB and MO from aqueous solution on TPP-NH$_2$

[a]School of Chemistry and Molecular Engineering, East China University of Science and Technology, Shanghai, 200237, China. E-mail: cjpeng@ecust.edu.cn; Tel: +86-21-64252630

[b]Environmental Protection Key Laboratory of Environmental Risk Assessment and Control on Chemical Process, East China University of Science and Technology, Shanghai, 200237, China. E-mail: qyang@ecust.edu.cn; Tel: +86-21-64252748

were studied in detail. The fast adsorption kinetics, large adsorption capacity, excellent physicochemical stability and good reusability make TPP-NH$_2$ a highly attractive adsorbent for the removal of organic dyes and solvents from aqueous solution.

2. Experimental

2.1 Reagents and materials

All of the purchased chemicals were of at least reagent grade and were used without further purification. Triptycene (98.0%), anhydrous ferric chloride (FeCl$_3$, ≥98.0%), 1,2-dichloroethane (DCE, 99.8%) and formaldehyde dimethyl acetal (FDA, ≥98.0%) were purchased from Sigma-Aldrich. All of the other solvents were purchased from TCI America.

2.2 Synthesis of TPP-NH$_2$

TPP-NH$_2$ was synthesized according to our previous work.[17] As shown in Scheme 1, 14-aminotriptycene[19] monomer (20 mmol) was dissolved in 20 mL of anhydrous DCE. To this solution, dimethoxymethane (FDA, 80 mmol) and anhydrous FeCl$_3$ (80 mmol) were added under a nitrogen environment. The resulting reaction mixture was heated to 80 °C for 24 h with constant stirring. After cooling to room temperature, the crude product was collected *via* filtration and repeatedly washed with methanol until the filtrate was nearly colourless. The product was further purified *via* Soxhlet extraction in methanol for 24 h. Finally, the product was dried at 120 °C under vacuum to give a brown solid, TPP-NH$_2$.

2.3 Instruments and characterization

The morphology of the samples was characterized using a Nova NanoS 450 field emission scanning electron microscope (FE-SEM). Transmission electron microscope (TEM) and high-resolution transmission electron microscope (HRTEM) images were recorded on a JEM-2100 transmission electron microscope. The powder samples were treated in ethanol using ultrasound for 20 min and were then dropped and dried on carbon-coated copper grids. The powder X-ray diffraction (XRD) data were collected on a D/Max2550 VB/PC diffractometer (40 kV, 200 mA) using Cu Kα radiation. The N$_2$ adsorption–desorption isotherms were measured at 77 K using a volumetric adsorption analyzer Micromeritics ASAP 2020. Before taking the

adsorption measurements, the samples were degassed at 120 °C for 24 h. The specific surface areas were calculated using the Brunauer–Emmett–Teller (BET) method and the Langmuir method. The total volume was calculated at $p/p_0 = 0.99$. The micropore volume was derived from the t-plot method.

2.4 Adsorption test

Organic dye adsorption.[20] 10 mg of porous polymer TPP-NH$_2$ was added to 50 mL of MEB and MO solution with an initial concentration from 1 ppm to 1000 ppm under mechanical shaker conditions at a predetermined temperature ($T = 30$ °C, 40 °C, 50 °C) for 12 h. The residual concentration of the dyes was determined at the maximum wavelength (464 nm for MO and 664 nm for MEB) using UV-vis spectroscopy. The adsorption capacities and removal percentages of the dyes were calculated using the following equations:

$$q_e = \frac{(C_0 - C_e) \times V}{m} \quad (1)$$

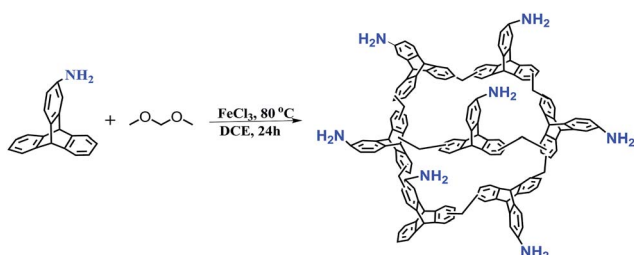$$E\% = \frac{(C_0 - C_e)}{C_0} \times 100\% \quad (2)$$

where q_e and $E\%$ denote the adsorption capacity (mg g^{-1}) and removal percentage of the metal ions, respectively; C_0 and C_e are the initial and equilibrium concentrations (mg L^{-1}) of the metal ions in aqueous solution, respectively; V is the volume of adsorption solution (mL); and m is the weight of the adsorbent (mg).

Organic dye adsorption kinetics. 10 mg of porous polymer TPP-NH$_2$ was added to 50 mL of MEB and MO solution with an initial concentration of 3 ppm under mechanical shaker conditions at 30 °C. After adsorption for a predetermined time (from 1 min to 540 min), the mixture was filtered with a 0.22 μm Millipore hydrophobic PTFE membrane, and the filtrate was measured using UV-vis spectroscopy.

pH effect on MEB and MO adsorption. The pH was adjusted using 0.1 M NaOH and 0.1 M HCl. The value of the pH was ranged from 2 to 9. Then, 10 mg of porous polymer TPP-NH$_2$ was added to 50 mL of a 1 ppm MEB and 3 ppm MO solution, with different pH values, at 30 °C.

Desorption experiments and reusability of TPP-NH$_2$. The adsorption/desorption cycles were conducted as follows: each adsorption experiment consisted of 50 mg of TPP-NH$_2$ with 250 mL of 1 ppm MEB and 3 ppm MO solution for 12 h. After the adsorption experiments, the dye-loaded powder in the flask was collected using filtration, washed with deionized water and stirred in water/ethanol for 24 h to desorb the dyes. The regeneration adsorbent was then filtered and separated from the solution, and washed with deionized water. Finally, the regeneration adsorbent was dried at 120 °C under vacuum. The desorption efficiency was calculated as the percentage of the mass of the analyte in the dyes desorbed to the elution medium of the total mass of the analyte adsorbed on the adsorbent. The above cycle was repeated 5 times.

Organic solvent adsorption. Six different kinds of organic solvent, including chloroform, dichloromethane, toluene, methanol, petroleum ether, and ethanol, were used in this

Scheme 1 Schematic representation of the synthesis of the amine functionalized polymer TPP-NH$_2$.

study, and water was also used as a contrast. For example, in a typical adsorption experiment that used chloroform, a certain amount of TPP-NH$_2$ was weighed (w_1) and put in a small piece of glass tubing using adsorbent cotton at room temperature, and then the tube was fully immersed in chloroform overnight. A weight measurement (w_2) was done immediately after taking it out from the solvent to avoid evaporation. The adsorption capacity value, W_t (w/w)% ($W_t\% = 100(w_2 - w_1)/w_1$), was thus calculated. Other solvent adsorption experiments were done in the same way.

3. Results and discussion

3.1 Characterization of TPP-NH$_2$

The synthesized TPP-NH$_2$ was characterized using SEM, HRTEM, XRD and N$_2$ adsorption–desorption. The SEM image (Fig. 1a) shows the solid sphere morphology of the sub-micrometer particles in TPP-NH$_2$. The HRTEM image (Fig. 1b) shows that TPP-NH$_2$ possesses a large amount of amorphous microporosity. In addition, with a broad band from 10° to 35° in the XRD pattern (Fig. 1c), it confirmed the amorphous nature of TPP-NH$_2$. The porosity of the TPP-NH$_2$ was evaluated using the nitrogen adsorption–desorption isotherm measurements at 77 K. As shown in Fig. 1d, the initial sharp increase in the uptake at low pressures ($p/p_0 < 0.1$) is characteristic of type I isotherms, *i.e.*, TPP-NH$_2$ has significant microporous character. The hysteresis loops up to relative pressures above 0.9 suggest the occurrence of macropores and interparticle voids. The presence of minimal hysteresis in the N$_2$ desorption curves of these polymers suggests partial mesoporous character. In microporous polymers, this behaviour is usually ascribed to the swelling effects of the polymer networks while coming into contact with the adsorbate gas and expanded networks of 3D rigid building blocks.

The BET specific surface area of TPP-NH$_2$ measured from the nitrogen isotherms was 863 m^2 g^{-1}. The pore size distribution

(PSD) curve (Fig. 1d (inset)), calculated based on non-local density functional theory (NLDFT), also confirmed the presence of primary micropores and a few mesopores, which can also be observed in some other polymers derived from using the "knitting" approach.[14]

3.2 Adsorption kinetics of MEB and MO on TPP-NH$_2$

The time-dependent adsorption of MEB and MO on TPP-NH$_2$ was investigated at an initial concentration of 3 ppm. As shown in Fig. 2a and c, the removal percentage increased sharply within 60 min and slowed down thereafter, and, finally, reached equilibrium. It is worth mentioning that more than 95% of both dyes could be removed from the aqueous solution within 60 min at room temperature, indicating that the charge of the dyes plays no significant role in the kinetics of the adsorption. As the adsorption time went on, the adsorption intensities of the MEB and MO aqueous solution became weaker (Fig. 2b and d). Therefore, the optimum contact time was considered to be 60 min.

It was reported that more than 120 min is needed to attain equilibrium for dyes with several adsorbents, such as magnetic cellulose beads,[21] porous chromium benzenedicarboxylates (Cr-BDC),[22] and a mesoporous hybrid xerogel.[23] In contrast, in the present study, the percentage removal of dyes on TPP-NH$_2$ was very high (>95%) in a short amount of time. Therefore, fast adsorption is observed for TPP-NH$_2$, which can be attributed to its large surface area and hierarchical porosity.

Furthermore, the adsorption data are fitted with a pseudo-second-order kinetic model (eqn (3)) (Fig. 2e and f).

$$\frac{t}{q_t} = \frac{1}{k_2 q_e^2} + \frac{t}{q_e} \tag{3}$$

where q_t and q_e are the adsorption capacity (mg g^{-1}) at a certain time t (min) and equilibrium, respectively, and k_2 is the rate
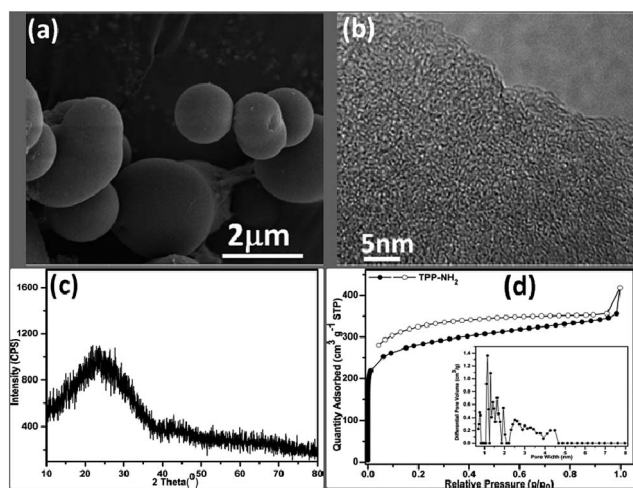

Fig. 1 (a) SEM, (b) HRTEM, (c) XRD and (d) N$_2$ adsorption–desorption isotherms and pore size distributions (the inset of (d)) of TPP-NH$_2$ at 77 K.
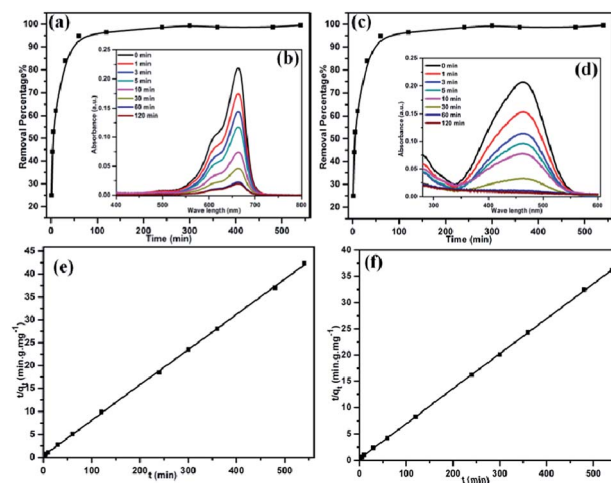

Fig. 2 The MEB (a) and MO (c) adsorption on the polymer TPP-NH$_2$ at different times. The insets show the UV-vis adsorption spectra of MEB (b) and MO (d). The plots of the pseudo-second-order kinetics for the adsorption of MEB (e) and MO (f) (MEB concentration: 3 ppm and MO concentration: 3 ppm).

constant for the pseudo-second-order adsorption (g mg^{-1} min^{-1}). An extremely high correlation coefficient ($R^2 > 0.999$) is obtained for the pseudo-second-order kinetic model (Table 1). This suggests that the rate of adsorption of the organic dyes on the TPP-NH$_2$ adsorbent depends on the availability of adsorption sites.

3.3 Effect of pH on the adsorption of MEB and MO on TPP-NH$_2$

The effect of the pH on the adsorption of MEB and MO was studied in the pH range 2 to 9 (Fig. 3). The percentage removal of MEB on TPP-NH$_2$ was almost unchanged as the pH increased. However, a lower percentage of MO was observed at pH 2–3. The MO molecule was present in the solution as quinone and azo structures (pK_a = 3.47, Scheme 2), depending on the solution pH.[24] It is predicted that the azo structure should have a more conjugated π system[25] than its quinone counterpart. Indeed, the adsorption capacity for MO under basic conditions was found to be higher than that under acidic conditions, predicting the role of π–π stacking interactions in the dye adsorption on TPP-NH$_2$. The above results show that the electrostatic interaction is not the main mechanism involved in the efficient adsorption of MEB and MO. The efficient adsorption performance of 3D TPP-NH$_2$ was attributed to its good porosity and high surface area, as well as the π–π stacking interactions between the aromatic rings of MEB and MO and the aromatics rings in the chain of TPP-NH$_2$.

3.4 Adsorption isotherms of MEB and MO on TPP-NH$_2$

The adsorption isotherms were studied at three different temperatures (30–50 °C) in the initial concentration range 1–1000 ppm (Fig. 4). The adsorption capacity of MEB and MO increased with the initial concentration of MEB and MO, indicating favorable adsorption of MEB and MO on TPP-NH$_2$ at high concentrations. To evaluate the maximum adsorption capacity of MEB and MO, the adsorption isotherms were fitted using the Langmuir model (eqn (4)):[26]

$$\frac{C_e}{q_e} = \frac{C_e}{q_{max}} + \frac{1}{q_{max}b} \tag{4}$$

where C_e is the equilibrium concentration (mg L^{-1}) of the dyes, q_e is the equilibrium adsorption capacity (mg g^{-1}) of the dyes, q_{max} is the maximum adsorption capacity (mg g^{-1}), and b is the Langmuir constant. The plots of C_e/q_e against C_e gave good linear plots at all of the test initial concentrations, indicating the adsorption of MEB and MO follows the Langmuir model
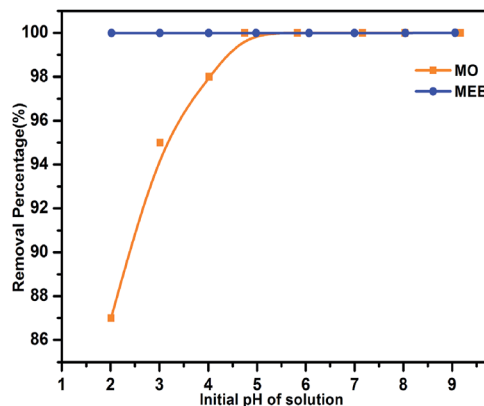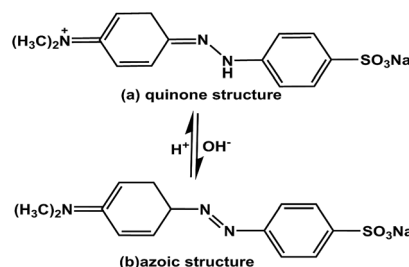

Fig. 3 Effect of pH on the adsorption of MEB (blue) and MO (orange) (MEB concentration: 1 ppm and MO concentration: 3 ppm).

(Fig. 4c and d). The maximum adsorption capacity increased from 204.9 mg g^{-1} to 560.6 mg g^{-1} and 213.2 mg g^{-1} to 803.2 mg g^{-1} for MEB and MO, respectively, as the temperature increased, suggesting the adsorption of MEB and MO on TPP-NH$_2$ is favourable at high temperatures *via* an endothermic process.[27–29] Compared to the other reported adsorbent polymers,[21,25,27,28,30–34] summarized in Table 2, the adsorption capacity of the TPP-NH$_2$ adsorbent for MEB and MO make it one of the most promising adsorbents. Therefore, this novel 3D TPP-NH$_2$ adsorbent can be recommended as an efficient alternative for dye removal.

3.5 Desorption and regeneration of TPP-NH$_2$

The pH studies and adsorption isotherms suggest that TPP-NH$_2$ is an efficient MEB and MO adsorber owing to its good porosity, high surface area and the π–π stacking interactions between dyes and TPP-NH$_2$, which indicate that the MEB and MO can be released from TPP-NH$_2$ by rinsing with water/ethanol. The desorption efficiency is up to 94%. To demonstrate the reusability of the TPP-NH$_2$ adsorbent, an adsorption–desorption cycle was repeated five times. As Fig. 5 shows, the adsorption capacity of the TPP-NH$_2$ adsorbent does not significantly change during the adsorption–desorption recycling. The results indicate that the TPP-NH$_2$ adsorbent is suitable for the efficient removal of dyes from aqueous solution.

Table 1 Pseudo-second-order kinetic parameters for the adsorption of MEB and MO at 30 °C

| Dyes | $q_{e(exp)}$ (mg g^{-1}) | Pseudo-second-order kinetic model | | |
		$q_{e(cal)}$ (mg g^{-1})	k_2 (g mg^{-1} min^{-1})	R^2
MEB	12.74	12.96	0.0059	0.999
MO	15.09	15.22	0.0043	0.999

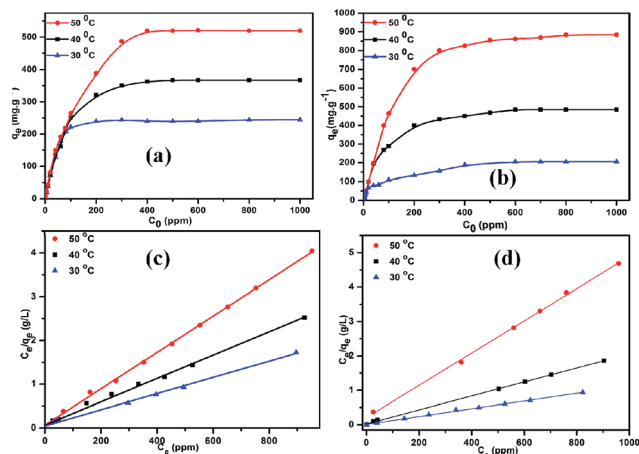**Scheme 2** Structures of methyl orange under acidic and alkaline conditions.

Fig. 4 Adsorption isotherms for the adsorption of MEB (a) and MO (b) on TPP-NH$_2$ in the temperature range 30–50 °C and the corresponding Langmuir plots for MEB (c) and MO (d).

Table 2 Comparison of the maximum equilibrium adsorption capacity of the dyes on different adsorbents at room temperature

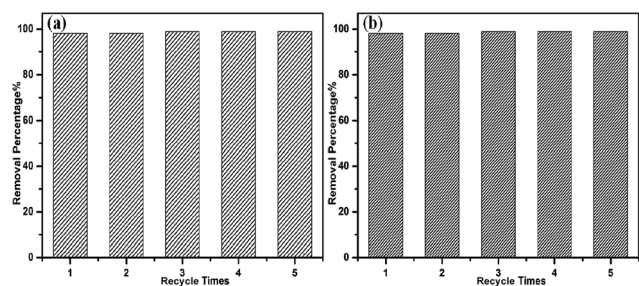| Adsorbents	q_{max} (mg g^{-1}) of different dyes		Ref.
	MEB	MO	
Magnetic cellulose beads	0.79	1.43	21
MOF-235	187	477	25
Activated carbon	11.2	26	25
MWCNTs	—	51.7	27
GNS–Fe$_3$O$_4$	43.08	—	28
Cellulose-based wastes	20.8	21	30
Porous carbon monoliths	127	—	31
CNTs-A	399	149	32
Hyper-cross-linked polymeric adsorbent	—	70	33
AGS	212	—	34
TPP-NH$_2$	204.9	213.2	This work

Fig. 5 Reusability of the polymer TPP-NH$_2$ for removing MEB (a) and MO (b).

3.6 Adsorption of the organic solvents on TPP-NH$_2$

In addition to the dye adsorption capacity, a high organic solvent adsorption capacity is also essential for water treatment.
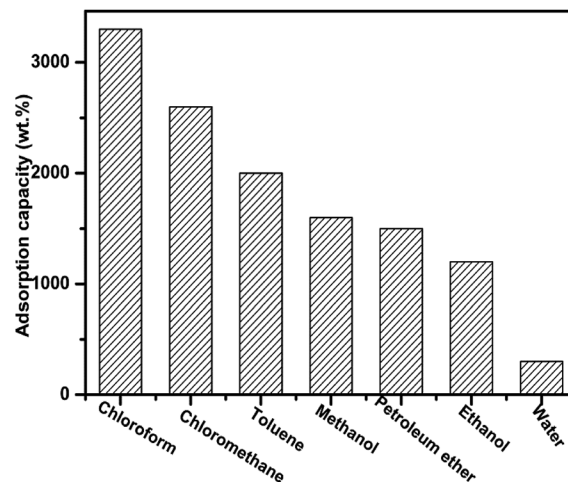

Fig. 6 Adsorption capacity of TPP-NH$_2$ for different organic solvents.

As shown in Fig. 6, the adsorption values of the organic solvents were in the range 1100–3300 wt%, while TPP-NH$_2$ only uptook less than 100 wt% of water. The organic solvent adsorption capacities on TPP-NH$_2$ show the sequence chloroform (3300 wt%) > chloromethane (2600 wt%) > toluene (2000 wt%) > methanol (1600 wt%) > petroleum ether (1505 wt%) > ethanol (1380 wt%) > water (85 wt%), which is a little different to the sequence of their polarities. The above results show that the difference in polarity of the organic solvents is not the only decisive factor involved in the efficient adsorption of the organic solvents. The excellent performance of TPP-NH$_2$ in adsorbing organic solvents might also be due to the hierarchical pores on TPP-NH$_2$.

4. Conclusions

An amine functionalized 3D porous organic polymer with a high surface area and good porosity was synthesized via a convenient and efficient Friedel–Crafts reaction. The obtained polymer TPP-NH$_2$ shows high adsorption capacities for organic dyes and solvents and thus can be used as an adsorbent to clean contaminated water. The ease of synthesis and low cost coupled with the efficient and rapid adsorption properties make TPP-NH$_2$ an attractive adsorbent for a wide range of large-scale applications in water purification and treatment.

Conflict of interest

The authors declare no competing financial interest.

Acknowledgements

References

1 V. K. Gupta and I. A. Suhas, *J. Environ. Manage.*, 2009, **90**, 2313–2342.

2 G. Crini, *Bioresour. Technol.*, 2006, **97**, 1061–1085.

3 J. Z. Suhong Chen, C. Zhang, Q. Yue, Y. Li and C. Li, *Desalination*, 2010, **252**, 149–156.

4 A. Mittal, A. Malviya, D. Kaur, J. Mittal and L. Kurup, *J. Hazard. Mater.*, 2007, **148**, 229–240.

5 M. Hartmann, S. Kullmann and H. Keller, *J. Mater. Chem.*, 2010, **20**, 9002.

6 M. M. Khin, A. S. Nair, V. J. Babu, R. Murugan and S. Ramakrishna, *Energy Environ. Sci.*, 2012, **5**, 8075.

7 A. Walcarius and L. Mercier, *J. Mater. Chem.*, 2010, **20**, 4478.

8 M. Rafatullah, O. Sulaiman, R. Hashim and A. Ahmad, *J. Hazard. Mater.*, 2010, **177**, 70–80.

9 G. Chen, N. Iyi and R. Sasai, *J. Mater. Res.*, 2002, **17**(05), 1035–1040.

10 Y. Zhou, Y. Wang, T. Liu, G. Chen and C. Yan, *Sci. Rep.*, 2017, **7**, 45065.

11 D. Mohan, K. P. Singh and V. K. Singh, *J. Hazard. Mater.*, 2008, **152**, 1045–1053.

12 E. Alver and A. Ü. Metin, *Chem. Eng. J.*, 2012, **200–202**, 59–67.

13 D. Wu, F. Xu, B. Sun, R. Fu, H. He and K. Matyjaszewski, *Chem. Rev.*, 2012, **112**, 3959–4015.

14 B. Li, R. Gong, W. Wang, X. Huang, W. Zhang, H. Li, C. Hu and B. Tan, *Macromolecules*, 2011, **44**, 2410–2414.

15 B. Li, Y. Zhang, D. Ma, Z. Shi and S. Ma, *Nat. Commun.*, 2014, **5**, 5537.

16 Y. Zhang and S. N. Riduan, *Chem. Soc. Rev.*, 2012, **41**, 2083–2094.

17 Y. He, X. Zhu, Y. Li, C. Peng, J. Hu and H. Liu, *Microporous Mesoporous Mater.*, 2015, **214**, 181–187.

18 D. O. K. F. Jiang, A. M. Spokoyny, B. G. Hauser, Y. Sang Bae, S. E. Brown, R. Q. Snurr, C. A. Mirkin and J. T. Hupp, *Chem. Mater.*, 2009, **21**, 3033–3035.

19 J. H. Chong and M. J. MacLachlan, *Inorg. Chem.*, 2006, **45**, 1442–1444.

20 Q. Li, J. Zhang, Q. Lu, J. Lu, J. Li, C. Dong and Q. Zhu, *Mater. Lett.*, 2016, **170**, 167–170.

21 X. Luo and L. Zhang, *J. Hazard. Mater.*, 2009, **171**, 340–347.

22 E. Haque, J. E. Lee and I. T. Jang, *J. Hazard. Mater.*, 2010, **181**(1), 535–542.

23 Z. Wu, H. Joo and K. Lee, *Chem. Eng. J.*, 2005, **112**, 227–236.

24 W. Cheah, S. Hosseini, M. A. Khan, T. G. Chuah and T. S. Y. Choong, *Chem. Eng. J.*, 2013, **215–216**, 747–754.

25 E. Haque, J. W. Jun and S. H. Jhung, *J. Hazard. Mater.*, 2011, **185**, 507–511.

26 E. Haque, J. W. Jun, S. N. Talapaneni, A. Vinu and S. H. Jhung, *J. Mater. Chem.*, 2010, **20**, 10801.

27 B. H. Yunjin Yao, F. Xu and X. Chen, *Chem. Eng. J.*, 2011, **170**, 82–89.

28 C. Z. Lunhong Aia and Z. Chen, *J. Hazard. Mater.*, 2011, **192**, 1515–1524.

29 J. Q. Jiang, C. X. Yang and X. P. Yan, *ACS Appl. Mater. Interfaces*, 2013, **5**, 9837–9842.

30 R.-S. J. Gurusamy Annadurai and D.-J. Lee, *J. Hazard. Mater.*, 2002, **B92**, 263–274.

31 X. He, K. B. Male, P. N. Nesterenko, D. Brabazon, B. Paull and J. H. Luong, *ACS Appl. Mater. Interfaces*, 2013, **5**, 8796–8804.

32 J. Ma, F. Yu, L. Zhou, L. Jin, M. Yang, J. Luan, Y. Tang, H. Fan, Z. Yuan and J. Chen, *ACS Appl. Mater. Interfaces*, 2012, **4**, 5749–5760.

33 J.-H. Huang, K.-L. Huang, S.-Q. Liu, A. T. Wang and C. Yan, *Colloids Surf., A*, 2008, **330**, 55–61.

34 F. Liu, S. Teng, R. Song and S. Wang, *Desalination*, 2010, **263**, 11–17.